Accuracy of transport models for waves in random media

Guillaume Bal

Department of Applied Physics and Applied Mathematics, Columbia University, New York NY, 10027

Olivier Pinaud

Department of Applied Physics and Applied Mathematics, Columbia University, New York NY, 10027

Abstract

This paper addresses the validity of radiative transfer equations as a model for the energy density of waves propagating in highly heterogeneous media. Comparisons between acoustic wave simulations over domains of size comparable to 500 wavelength in two space dimensions and Monte Carlo simulations of radiative transfer equations are performed. In the so-called weak coupling regime, the agreement between the energy densities obtained by solving the wave equations and those predicted by solving the radiative transfer equations is remarkable. The domain of validity of the radiative transfer equations is assessed by looking at the fluctuations in the energy density they predict in the presence of small-volume defects in the underlying media.

Key words: High frequency wave equations, weak-coupling regime, radiative transfer equations, random media, numerical simulations.

1 Introduction

The energy density or probability density of high frequency waves propagating in highly heterogeneous media has long been modeled by radiative transfer equation in many fields: quantum

Email addresses: gb2030@columbia.edu (Guillaume Bal), op2102@columbia.edu (Olivier Pinaud).

URL: www.columbia.edu/∼gb2030 (Guillaume Bal).

waves in semiconductors, electromagnetic waves in turbulent atmospheres and plasmas, microwaves in aerial communication, underwater acoustic waves, elastic waves in the Earth's crust. The derivation of such kinetic models may either be phenomenological or based on first principles for the wave fields; see e.g. [12,15,19,20,23,25,27,28,31] in the physical literature and [3,18,26,30] in the mathematical literature. The latter references derive the equations of radiative transfer in the regime of wave propagation called the *weak coupling* regime, whereby waves propagate over distances that are large compared to the typical wavelength in the system and the fluctuations have weak amplitude and correlation length comparable to the wavelength.

However, very little exists on the validity of the radiative transfer equations in the weak coupling regime, and the comparison of energy densities obtained by solving for the wave fields with those obtained by solving the radiative transfer equations. The main contribution of this paper is to assess the predictive power of the radiative transfer equation in domains that are very large compared to the typical wavelength in the system. The wave energy density is calculated by solving numerically a first-order system of acoustic equations in the time domain. The radiative transfer equations are then solved by a Monte Carlo method based on the probabilistic representation of transport equations, and the two energies are compared as a function of time at some physical position in the domain where detectors are located. The well-documented diffusive approximation to radiative transfer, which arises in the limit of large domains relative to the mean free path, is also considered and solved numerically by a finite element method.

Typically, the constitutive parameters of the radiative transfer model, i.e., primarily the mean free path and the transport mean free path, are estimated theoretically based on the statistical properties of the underlying heterogeneous medium, and then estimated numerically by considering the best radiative transfer fit to the energy calculated by solving the system of acoustic equations. We will show that these two estimates of the constitutive parameters agree quite well for several statistics of the underlying media. Once these spatially homogeneous parameters are obtained, we wish to assess the spatial resolution of the radiative transfer predictions. This is done as follows. The statistically homogeneous underlying medium is perturbed locally by a small inclusion with different statistical properties from the background medium. We consider void inclusions, where the heterogeneous fluctuations of the underlying medium are suppressed, and perfectly reflecting inclusions, at the surface of which energy is specularly reflected. We then compare the influence of the small inclusion on the energy densities obtained by the wave simulation and the radiative transfer simulation.

We will see that not-too-small inclusions generate energy density fluctuations that are above the noise level generated by the random oscillations in the underlying medium and are well-predicted by the radiative transfer theory. The influence of smaller inclusions may however be too faint to be distinguished from fluctuations generated by the random oscillations. In that case, the energy estimates predicted by the radiative transfer equation fail to be sufficiently stable statistically to be of any use. Such energy estimates may still be valid to predict the *average* influence of the inclusion, i.e., after averaging over all possible realizations of the heterogeneous medium with given statistics is performed. This is not what we are interested in in this paper. We want to understand the predictive power of radiative transfer to detect local fluctuations for one "typical" realization of the underlying medium. In some sense we are interested in quantifying the *statistical stability* of the wave energy density in the weak

coupling regime. We refer the reader to [2,7,10,24] for works on the statistical stability of the energy density of classical waves in random media.

The rest of the paper is constructed as follows. Section 2 recalls the radiative transfer equations for acoustic waves and for discretized acoustic waves. The latter results allow us to estimate the modifications in the kinetic parameters generated by the discretization of the wave equation. The numerical tools used in the comparisons are presented in section 3. The wave equation is simulated by a finite difference forward in time algorithm implemented on parallel architectures. The transport equation is solved by Monte Carlo, whereas its diffusion approximation is solved by the finite element method. Finally, our numerical results on the comparison of the energy densities obtained by the various solvers are gathered in section 4. Some conclusions are offered in section 5.

2 Kinetic models for wave propagation

In this section, we recall the derivation of radiative transfer equations following references [3,26]. Written as a symmetric first-order system, the equation for the pressure $p(t,\mathbf{x})$ and the velocity field $\mathbf{v}(t,\mathbf{x})$ takes the form

$$\rho(\mathbf{x})\frac{\partial \mathbf{v}}{\partial t} + \nabla p = 0, \qquad \kappa(\mathbf{x})\frac{\partial p}{\partial t} + \nabla \cdot \mathbf{v} = 0, \qquad p(0,\mathbf{x}) = p_0(\mathbf{x}), \quad \mathbf{v}(0,\mathbf{x}) = \mathbf{v}_0(\mathbf{x}), \tag{1}$$

where $\rho(\mathbf{x})$ is density and $\kappa(\mathbf{x})$ compressibility of the underlying media. Here, $t > 0$ and $\mathbf{x} \in \mathbb{R}^d$, where $d \geq 2$ is spatial dimension. We will only consider propagating initial conditions and thus assume the existence of a pressure potential $\phi(\mathbf{x})$ such that $\rho(\mathbf{x})\mathbf{v}_0(\mathbf{x}) = -\nabla\phi(\mathbf{x})$. This prevents the presence of vortical modes [3,26] in the system.

The numerical simulations presented in this paper are for $d = 2$. The above system is the starting point for the derivation of kinetic models in e.g. [3,25,26], whose role is to describe the spatial distribution of the wave energy density, which, averaged over the whole domain, is a conserved quantity:

$$\mathcal{E}(t) = \frac{1}{2}\int_{\mathbb{R}^d} \Big(\rho(\mathbf{x})|\mathbf{v}|^2(t,\mathbf{x}) + \kappa(\mathbf{x})p^2(t,\mathbf{x})\Big)d\mathbf{x} = \mathcal{E}(0). \tag{2}$$

Although this is by no means necessary in the derivation of kinetic equations, we shall assume in the sequel that $\rho = \rho_0$ is constant.

High Frequency Regime. Kinetic models arise in the high frequency limit of wave propagation. We consider the framework where the typical distance of propagation L of the waves is much larger than the typical wavelength λ in the system. We introduce the small adimensionalized parameter

$$\varepsilon = \frac{\lambda}{L} \ll 1.$$

When $\varepsilon \approx 1$, the energy density of waves is obtained by simply solving the wave equation. In the high frequency regime, we rescale $t \to \varepsilon^{-1}t$ and $\mathbf{x} \to \varepsilon^{-1}\mathbf{x}$ and obtain the following

equation for $\mathbf{u}_\varepsilon = (\mathbf{v}_\varepsilon, p_\varepsilon)$:

$$\rho_0 \varepsilon \frac{\partial \mathbf{v}_\varepsilon}{\partial t} + \varepsilon \nabla p_\varepsilon = 0, \quad \kappa_\varepsilon(\mathbf{x}) \varepsilon \frac{\partial p_\varepsilon}{\partial t} + \varepsilon \nabla \cdot \mathbf{v}_\varepsilon = 0, \quad p_\varepsilon(0,\mathbf{x}) = p_{0\varepsilon}(\mathbf{x}),\ \mathbf{v}_\varepsilon(0,\mathbf{x}) = \mathbf{v}_{0\varepsilon}(\mathbf{x}), \quad (3)$$

where the initial conditions $p_{0\varepsilon}(\mathbf{x})$ and $\mathbf{v}_{0\varepsilon}(\mathbf{x})$ oscillate at the frequency ε^{-1}. Typically we consider initial conditions of the form $\phi(\mathbf{x})\cos(\varepsilon^{-1}\boldsymbol{\xi}\cdot\mathbf{x})$ for a given $\boldsymbol{\xi} \in \mathbb{R}^d$, and more specifically in our numerical simulations, isotropic superpositions of such initial conditions; see (21) below.

Energy conservation is written in the form

$$\mathcal{E}_\varepsilon(t) = \frac{1}{2}\int_{\mathbb{R}^d} \Big(\rho_0 |\mathbf{v}_\varepsilon|^2(t,\mathbf{x}) + \kappa_\varepsilon(\mathbf{x}) p_\varepsilon^2(t,\mathbf{x})\Big) d\mathbf{x} = \mathcal{E}_\varepsilon(0). \quad (4)$$

We now present a kinetic theory that models the spatial distribution of the energy described in the above conservation law.

Radiative Transfer model in weak coupling regime. We assume that the medium is characterized by a compressibility of the form

$$\kappa_\varepsilon(\mathbf{x}) = \kappa_0(\mathbf{x}) + \sqrt{\varepsilon}\kappa_1\Big(\mathbf{x}, \frac{\mathbf{x}}{\varepsilon}\Big), \quad (5)$$

where $\kappa_0(\mathbf{x})$ is the average background compressibility, and $\kappa_1(\mathbf{x},\mathbf{y})$ models the random fluctuations. The variable $\mathbf{y}$ corresponds to the small scale variations and the variable $\mathbf{x}$ to the large scale variations. For each $\mathbf{x} \in \mathbb{R}^d$, $\mathbf{y} \to \kappa_1(\mathbf{x},\mathbf{y})$ is a mean-zero statistically homogeneous random field. Note that the compressibility fluctuations oscillate at the frequency ε^{-1}, as do the waves in the system. This regime, where the correlation length of the medium and the wavelength of the propagating waves are the same, thus maximizes interactions of the wave fields with the underlying medium.

The sound speed is given by

$$c_\varepsilon^2(\mathbf{x}) = \frac{1}{\rho_0 \kappa_\varepsilon(\mathbf{x})}. \quad (6)$$

We thus verify that up to negligible lower order terms (in the limit $\varepsilon \to 0$), we have

$$c_\varepsilon^2(\mathbf{x}) = c_0^2(\mathbf{x}) - \sqrt{\varepsilon} V(\mathbf{x}, \frac{\mathbf{x}}{\varepsilon}), \qquad V(\mathbf{x},\mathbf{y}) = \frac{c_0^2(\mathbf{x})}{\kappa_0(\mathbf{x})}\kappa_1(\mathbf{x},\mathbf{y}), \quad (7)$$

where $c_0(\mathbf{x}) = (\rho_0\kappa_0(\mathbf{x}))^{-1/2}$ is the background speed and $V(\mathbf{x},\mathbf{y})$ accounts for the random fluctuations.

The random inhomogeneities of the underlying medium are thus modeled by the functions $V(\mathbf{x},\mathbf{y})$. Inheriting the properties from the fluctuations in $\kappa_\varepsilon(\mathbf{x})$, we assume that for all $\mathbf{x}$, $V(\mathbf{x},\mathbf{y})$ is a statistically homogeneous mean-zero random field in the $\mathbf{y}$ variable. Moreover its two point statistics are known and the two-point correlation functions, or equivalently their Fourier transform the power spectra, are defined by

$$c_0^4(\mathbf{x}) R(\mathbf{x},\mathbf{z}) = \mathbb{E}\{V(\mathbf{x},\mathbf{y})V(\mathbf{x},\mathbf{y}+\mathbf{z})\} \quad (8)$$

$$(2\pi)^d c_0^4(\mathbf{x})\hat{R}(\mathbf{x},\mathbf{p})\delta(\mathbf{p}+\mathbf{q}) = \mathbb{E}\{\hat{V}(\mathbf{x},\mathbf{p})\hat{V}(\mathbf{x},\mathbf{q})\}. \quad (9)$$

Here, $\mathbb{E}\{\cdot\}$ denotes mathematical expectation, i.e., averaging over realizations of the random medium. The above power spectrum $\hat{R}(\mathbf{x},\mathbf{p})$ is the only statistical characteristic of the random medium that survives in the limit of high frequency, as $\varepsilon \to 0$. In this limit it is shown [3,25,26] that there exists a *phase-space* energy density $a(t,\mathbf{x},\mathbf{k})$ such that

$$\lim_{\varepsilon\to 0}\mathcal{E}(t) = \lim_{\varepsilon\to 0}\frac{1}{2}\int_{\mathbb{R}^d}\Big(\rho_0|\mathbf{v}_\varepsilon|^2(t,\mathbf{x}) + \kappa_\varepsilon(\mathbf{x})p_\varepsilon^2(t,\mathbf{x})\Big)d\mathbf{x} = \int_{\mathbb{R}^{2d}} a(t,\mathbf{x},\mathbf{k})d\mathbf{k}d\mathbf{x}. \tag{10}$$

More precisely, we have the local estimate

$$\lim_{\varepsilon\to 0}\frac{1}{2}\Big(\rho_0|\mathbf{v}_\varepsilon|^2(t,\mathbf{x}) + \kappa_\varepsilon(\mathbf{x})p_\varepsilon^2(t,\mathbf{x})\Big) = \int_{\mathbb{R}^d} a(t,\mathbf{x},\mathbf{k})d\mathbf{k}. \tag{11}$$

Thus $a(t,\mathbf{x},\mathbf{k})$ can be interpreted as an energy density in the phase space whose average over wavenumbers provides the spatial distribution of the energy density as a function of time. Moreover, the mode $a(t,\mathbf{x},\mathbf{k})$ solves the following radiative transfer equation

$$\frac{\partial a}{\partial t} + \nabla_{\mathbf{k}}\omega\cdot\nabla_{\mathbf{x}}a - \nabla_{\mathbf{x}}\omega\cdot\nabla_{\mathbf{k}}a + \Sigma(\mathbf{x},\mathbf{k})a = \int_{\mathbb{R}^d}\sigma(\mathbf{x},\mathbf{k},\mathbf{q})a(t,\mathbf{x},\mathbf{q})\delta\Big(\omega(\mathbf{x},\mathbf{q}) - \omega(\mathbf{x},\mathbf{k})\Big)d\mathbf{q}, \tag{12}$$

where $\omega(\mathbf{x},\mathbf{k}) = c_0(\mathbf{x})|\mathbf{k}|$ is the dispersion relation, and

$$\begin{aligned}\Sigma(\mathbf{x},\mathbf{k}) &= \frac{\pi\omega^2(\mathbf{x},\mathbf{k})}{2(2\pi)^d}\int_{\mathbb{R}^d}\hat{R}(\mathbf{x},\mathbf{k}-\mathbf{q})\delta\Big(\omega(\mathbf{x},\mathbf{q}) - \omega(\mathbf{x},\mathbf{k})\Big)d\mathbf{q},\\ \sigma(\mathbf{x},\mathbf{k},\mathbf{q}) &= \frac{\pi\omega^2(\mathbf{x},\mathbf{k})}{2(2\pi)^d}\hat{R}(\mathbf{x},\mathbf{k}-\mathbf{q}).\end{aligned} \tag{13}$$

Here, $\sigma(\mathbf{x},\mathbf{k},\mathbf{q})$ is the scattering coefficient and $\Sigma(\mathbf{x},\mathbf{k})$ the total absorption (extinction) coefficient. As waves propagate through the random medium, scattering occurs and this results in a macroscopic change in the direction of propagation. How this change of wavenumbers occurs is characterized locally by the scattering coefficient $\sigma(\mathbf{x},\mathbf{k},\mathbf{q})$. Note that the scattering operator is elastic, so that energy is conserved through scattering: the frequency $\omega(\mathbf{x},\mathbf{q})$ before scattering is equal to the frequency $\omega(\mathbf{x},\mathbf{k})$ after scattering. Since $\omega(\mathbf{x},\mathbf{k})$ is conserved by both the scattering operator and the advection term $\nabla_{\mathbf{k}}\omega\cdot\nabla_{\mathbf{x}}a - \nabla_{\mathbf{x}}\omega\cdot\nabla_{\mathbf{k}}a$, we deduce that equations for $a(t,\mathbf{x},\mathbf{k})$ at different values of ω are uncoupled. More specifically, when $c_0(\mathbf{x}) = c_0$ is a constant, we observe that equations for $a(t,\mathbf{x},\mathbf{k})$ at different values of $|\mathbf{k}|$ are uncoupled. At fixed ω, the above equation thus depends on $1+d+(d-1) = 2d$ variables in $d-$space variables. In the numerical simulations considered in this paper, where $d = 2$ and c_0 is constant, we thus have to solve 4-dimensional kinetic models for each fixed frequency ω.

The above kinetic equation need be augmented by a prescribed initial condition, which depends on the Wigner transform of the initial conditions $p_\varepsilon(0,\mathbf{x}) = p_0(\mathbf{x},\frac{\mathbf{x}}{\varepsilon})$ and $\mathbf{v}_\varepsilon(0,\mathbf{x}) = \mathbf{v}_0(\mathbf{x},\frac{\mathbf{x}}{\varepsilon})$, where to ensure that only propagating modes are generated $\mathbf{v}_0(\mathbf{x},\mathbf{y})$ assumes the form $\varphi(\mathbf{x})\nabla\phi(\mathbf{y})$ for smooth functions $\varphi(\mathbf{x})$ and $\phi(\mathbf{y})$. Following [26, (3.41)], the transport initial conditions take the form

$$a_0(\mathbf{x},\mathbf{k}) = \lim_{\varepsilon\to 0}\frac{1}{(2\pi)^d}\int_{\mathbb{R}^d} e^{i\mathbf{k}\cdot\mathbf{y}} f_\varepsilon(\mathbf{x},\mathbf{x}-\varepsilon\frac{\mathbf{y}}{2},\mathbf{k})f_\varepsilon^*(\mathbf{x},\mathbf{x}+\varepsilon\frac{\mathbf{y}}{2},\mathbf{k})d\mathbf{y}, \tag{14}$$

where

$$f_\varepsilon(\mathbf{x},\mathbf{y},\mathbf{k}) = \sqrt{\frac{\rho_0}{2}}\varphi(\mathbf{x})\nabla\phi(\mathbf{y})\cdot\hat{\mathbf{k}} + \sqrt{\frac{\kappa_0(\mathbf{x})}{2}}p_0(\mathbf{x},\mathbf{y}). \tag{15}$$

We refer to (23) below for the initial conditions corresponding to the numerical simulations presented in this paper.

Diffusion approximation. The radiative transfer equations are referred to in the physical literature as a mesoscopic regime, intermediate between the microscopic wave equation and the macroscopic diffusion equation. Mathematically, diffusion arises as the long-time large-distance limit of the radiative transfer equation [17,21,26]. Let us define the mean free path as $l = c_0/\Sigma$, where Σ is a typical value taken by $\Sigma(\mathbf{x},\mathbf{k})$ in (13) and c_0 is the average sound speed, assumed constant to simplify. The diffusive regime arises when the ratio $\eta = l/L \ll 1$. If time and space are rescaled as $t \to t/\eta^2$ and $\mathbf{x} \to \mathbf{x}/\eta$, we obtain in the limit that the propagating mode $a(t,\mathbf{x},\mathbf{k})$ is independent of the direction of propagation:

$$a(t,\mathbf{x},\mathbf{k}) \approx U(t,\mathbf{x},|\mathbf{k}|),$$

where we have in dimension $d = 2, 3$:

$$\begin{aligned} &\frac{\partial U}{\partial t} - \nabla\cdot D(\mathbf{x},|\mathbf{k}|)\nabla U = 0 \\ &U(0,\mathbf{x},|\mathbf{k}|) = \frac{c_0}{C_d|\mathbf{k}|^{d-1}}\int_{\mathbb{R}^d} a(0,\mathbf{x},\mathbf{p})\delta(c_0(|\mathbf{k}|-|\mathbf{p}|))d\mathbf{p}. \end{aligned} \tag{16}$$

Here $C_2 = 2\pi$ and $C_3 = 4\pi$ is the measure of the unit sphere. The diffusion coefficient is given by

$$D(\mathbf{x},|\mathbf{k}|) = \frac{c_0^2}{d[\Sigma(\mathbf{x},|\mathbf{k}|) - \lambda(\mathbf{x},|\mathbf{k}|)]} = \frac{c_0 l^*(\mathbf{x},|\mathbf{k}|)}{d}, \tag{17}$$

where the anisotropy factor λ is given via the relation [26]

$$\lambda(\mathbf{x},|\mathbf{k}|)\hat{\mathbf{k}} = \frac{c_0^2|\mathbf{k}|^2}{4(2\pi)^{d-1}}\int_{\mathbb{R}^d}\hat{R}(\mathbf{x},\mathbf{p}-\mathbf{k})\hat{\mathbf{p}}\delta(c_0(|\mathbf{k}|-|\mathbf{p}|))d\mathbf{p}, \tag{18}$$

and where the *mean free path* and the *transport mean free path*, which are characteristic distances of wave propagation in random media, are given by

$$l(\mathbf{x},|\mathbf{k}|) = \frac{c_0}{\Sigma(\mathbf{x},|\mathbf{k}|)}, \qquad l^*(\mathbf{x},|\mathbf{k}|) = \frac{c_0}{\Sigma(\mathbf{x},|\mathbf{k}|) - \lambda(\mathbf{x},|\mathbf{k}|)}, \tag{19}$$

respectively. The first distance l measures the main distance between successive interactions of the wave energy with the underlying media, whereas the second distance l^* measures the main distances it takes for the energy density to substantially change its direction of propagation. In anisotropic media, l^*, which is proportional to the diffusion coefficient, can be substantially larger than in isotropic media, which are characterized by $\lambda(\mathbf{x},|\mathbf{k}|) = 0$.

The main advantage of the diffusion approximation is that its solution is independent of the angular direction. Thus for a given frequency $\omega = c_0|\mathbf{k}|$, $U(t,\mathbf{x},|\mathbf{k}|)$ represents the spatial energy density as a function of time. Its numerical solution is therefore much faster than that of the full transport equation (12). We will see however that radiative transfer equations

provide a much more accurate estimate of the energy density than the diffusion approximation in the regime of moderate scattering. In the regime of large scattering (i.e., when propagation occurs over distances much larger than the mean free path), then the diffusion approximation becomes a very accurate description of the wave energy density.

Statistical stability. The derivation of (12) in [3,26] is based on formal arguments, which do not allow us to characterize the statistical stability of the transport solution $a(t, \mathbf{x}, \mathbf{k})$. What we mean by statistical stability is the invariance of the solution with respect to changes in the random media (in the fluctuations $V(\mathbf{x}, \mathbf{y})$) for given statistics in (9). The results obtained in [18,30] for the Schrödinger equation show that the ensemble average of the phase space energy density $\mathbb{E}\{a(t, \mathbf{x}, \mathbf{k})\}$ solves a kinetic equation. It remains to understand how small $a(t, \mathbf{x}, \mathbf{k}) - \mathbb{E}\{a(t, \mathbf{x}, \mathbf{k})\}$ is in practice.

Several mathematically rigorous results exist for transport models that are close to the radiative transfer equations mentioned above. In such models, such as the paraxial approximation of wave equations, the Itô-Schrödinger approximation of wave equations, or the regime of random Liouville equations, it is shown that the phase space energy density $a(t, \mathbf{x}, \mathbf{k})$ is indeed stable, at least in a weak sense (i.e., $a(t, \mathbf{x}, \mathbf{k})$ multiplied by an appropriate test function and integrated over an appropriate domain indeed is a deterministic variable). We refer the reader to [2,5,7,9,24] for additional details on the statistical stability of the wave energy density in these various regimes.

Statistical stability is a crucial aspect of the results we show in this paper. We want to assess the accuracy of the prediction obtained for the wave energy density by the radiative transfer model for *one* (typical) realization of the random medium, and not for an ensemble average of random media. Although the latter is also of interest, in practice one is often interested in the spatial distribution of the energy for one specific random medium, be it a given part of the Earth, the ocean, or the atmosphere. Although $a(t, \mathbf{x}, \mathbf{k})$ becomes statistically stable in the high frequency limit, this is only an approximation for a given non-zero wavelength, and only provided that sufficient spatial and angular averaging takes place.

On the one hand, sufficiently large variations in the macroscopic statistics of the random medium will generate modifications in the energy density that are above the level of statistical instabilities in the system. On the other hand, too small macroscopic variations that would be picked by the radiative transfer model in an ensemble average sense will cause modifications in the energy density that are below the noise created by microscopic statistical instabilities. How large the macroscopic fluctuations have to be in order to be detected on a "typical" realization of the random medium is addressed for specific examples in section 4.

3 Numerical setting

This section presents the numerical methods used to solve the different equations that describe wave propagation in random media. The wave and diffusion equations are discretized by using standard finite element methods on regular grids. Because the radiative transfer regime is a high frequency regime, the computational domain need be very large compared to the typical

wavelength in the system. Our calculations are performed on domains on the order of 500 wavelengths. The wave code has thus been implemented on parallel architectures to achieve sufficient accuracy (here, 20 points per wavelength). The radiative transfer equation has been solved by using a Monte-Carlo method.

The wave equation. The equations of acoustics are solved by using a second-order (both in space and time) mixed velocity-pressure formulation and a finite elements discretization on a regular grid [16]. A perfectly absorbing layer (a.k.a. perfectly matched layer or PML [13,14]) surrounds the domain Ω of interest (see Fig. 1 below). The spatial discretization of the continuous system (1) yields a semi-discrete linear system of the form:

$$M_V \frac{d\mathbf{V}}{dt} = R^t P, \qquad M_P \frac{dP}{dt} = -R\mathbf{V}, \tag{20}$$

for the semi-discrete pressure P and velocity $\mathbf{V}$, with appropriate initial conditions. The time variable in the latter system is discretized by a second-order centered scheme. By appropriate mass lumping [16], both mass matrices M_P and M_V are diagonal and the resulting scheme is second-order accurate. The initial condition is localized in the vicinity of a point $\mathbf{x}_0$ and at the same time has an oscillatory behavior at frequency $\mathbf{k}/\varepsilon$ (reduced frequency $\mathbf{k}$). In the simulations, the initial condition at wavenumber $\mathbf{k}_0$ is chosen to be

$$\mathbf{u}_0(\mathbf{x}) = \left(\mathbf{0}, C_0 \exp\left(\frac{-|\mathbf{x}-\mathbf{x}_0|^2}{2\sigma^2}\right) J_0(|\mathbf{k}_0||\mathbf{x}-\mathbf{x}_0|)\right)^t = (\mathbf{0}, p_0)^t, \tag{21}$$

where J_0 is the zero-th order Bessel function of the first kind. The constant C_0 is chosen such that the total energy (2) associated to $\mathbf{u}_0(\mathbf{x})$ equals 1. The Bessel function is an isotropic (i.e., uniformly weighted) superposition of plane waves with wavenumber $|\mathbf{k}_0|$. Typically σ is chosen to be on the order of ten wavelengths, where the "typical" wavelength in the system is $\lambda_0 = 2\pi/|\mathbf{k}_0|$ so that the frequency content of $\mathbf{u}_0$ is primarily that of a single wavenumber $|\mathbf{k}_0|$. The exponential term is here to localize the source term. It has sufficiently slow variations not to interfere with the main object of interest here, namely the highly oscillatory Bessel function. Note that the radiative transfer equations have constitutive parameters that depend on frequency. It is therefore important to ensure that only *one* frequency $\omega = c_0|\mathbf{k}|$ is present in the wave simulation to compare it with a kinetic model such as (12) at $\omega = c_0|\mathbf{k}|$ fixed. This is the main reason for the choice of initial conditions as in (21).

Other important choices in our numerical simulations are as follows. The width of the absorbing layers has been chosen to be $1.5\lambda_0$. We have observed that the amount of energy reflected by the PML was at most 10^{-4} times the energy of the initial conditions. It is therefore quite negligible. In all our simulations, we have assumed that

$$\rho_0 = 1, \quad \kappa(\mathbf{x}) = 1 + \sqrt{\varepsilon}\kappa_1\left(\frac{\mathbf{x}}{\varepsilon}\right), \tag{22}$$

where κ_1 is a stationary mean-zero random variable. The average sound speed is thus normalized to $c_0 = 1$. The fluctuations of the compressibility $\kappa_1(\mathbf{x})$ have been carefully modeled to satisfy prescribed power spectra in (9). This was done in the Fourier domain as in e.g. [11]. The parallelization of the wave code, otherwise written in the programming language c, has been performed by using the PETSc library, which considerably simplifies the message passing

procedure. The numerical simulations presented in the next section typically take several days each when they are performed on a (non-dedicated) cluster of 16 to 20 nodes.

The radiative transport equation. In the high frequency limit, we replace in the initial conditions (21) $|\mathbf{k}_0|$ by $|\mathbf{k}_0|/\varepsilon$ and σ by $\varepsilon\sigma_\varepsilon$. Assuming that $\varepsilon\sigma_\varepsilon \ll 1$ but that $\sigma_\varepsilon \gg 1$, we find (as in e.g. [22]) in the limit the following initial conditions for the kinetic model (12):

$$a_0(\mathbf{x},\mathbf{k}) = \delta(\mathbf{x}-\mathbf{x}_0)\delta(|\mathbf{k}|-|\mathbf{k}_0|)(2\pi|\mathbf{k}_0|)^{-1}. \tag{23}$$

Note that the energy emanates from one point, $\mathbf{x}_0$, at one frequency, $\omega = c_0|\mathbf{k}_0|$, and isotropically in directions. The energy is normalized so that $\int_{\mathbb{R}^2\times\mathbb{R}^2} a_0(\mathbf{x},\mathbf{k})d\mathbf{x}d\mathbf{k} = 1$. The radiative transfer equation (12) with the above initial conditions is solved by using a Monte Carlo method; see [29]. The probabilistic representation of transport equations shows that the solution to (12) is such that for all (Borel) subset $A \in \mathbb{R}^2$ and all (Borel) subset $B \in S^1$, the unit circle, we have that

$$\mathbb{P}\Big((\mathbf{X}(t),\mathbf{K}(t)) \in A\times B\Big) = \int_A\int_B a(t,\mathbf{x},|\mathbf{k}_0|\hat{\mathbf{k}})d\hat{\mathbf{k}}d\mathbf{x}, \tag{24}$$

where $\mathbb{P}$ denotes probability and the stochastic process $(\mathbf{X}(t),\mathbf{K}(t))$ is a jump process, which we now briefly describe. The initial condition $\mathbf{X}(0)$ is chosen at $\mathbf{X}(0) = \mathbf{x}_0$. The initial condition $\mathbf{K}(0)$ is chosen with uniform probability on the unit circle S^1. Then the particle moves freely, according to $\dot{\mathbf{X}}(t) = \mathbf{K}(t)$, for a random time given by an exponential law of parameter the total scattering coefficient Σ (see e.g. [29] for generalizations when the total scattering coefficient depends on space). At times t of scattering, the particle jumps from the direction $\mathbf{K}(t)$ to another direction $\mathbf{K}^+(t)$, where the probability of change of direction at $\mathbf{X}(t)$ from $\mathbf{K}$ to $\mathbf{K}^+$ is governed by the probability density $\sigma(\mathbf{X}(t),|\mathbf{k}_0|\mathbf{K}^+,|\mathbf{k}_0|\mathbf{K})/\Sigma(\mathbf{X}(t),|\mathbf{k}_0|)$. If at any time during the simulation, the particle exits the computational domain Ω, the particle's momentum $\mathbf{K}(t)$ is set to 0 so that the particle does not reenter the domain. This is consistent with the PML conditions imposed for the wave simulations.

In our simulations $B = S^1$ and A is the characteristic function of the detectors, equal to 1 where we have detectors and 0 elsewhere. The law of large numbers (the Monte Carlo method) is used to estimate (24) numerically by running N realizations of the above process independently. A very large number of particles, on the order of $N = 10^6$ in our simulations, is used to ensure that the statistical error (inversely proportional to the square root of the number of particles reaching the area $A\times B$) is sufficiently small.

Except for the presence of inclusions (see below) the random medium is statistically homogeneous. The mean free time $\Sigma^{-1} = l/c_0$ and the probability of jump to another direction after scattering described above thus are independent of the spatial position $\mathbf{x}$. As shown in (13), they depend however on the choice of a power spectrum for the random fluctuations of the compressibility κ_1, or equivalently of the sound speed V. We choose $\hat{R}$ to be of the form

$$\hat{R}(k) = \begin{cases} \hat{R}_0 & \text{for} \quad k < M, \\ 0 & \text{for} \quad k > M, \end{cases} \tag{25}$$

where M is a given parameter. The law of change of direction after scattering then simplifies as follows. Let us denote by $\Delta\theta$ the change in the direction of the particle after scattering,

i.e., if $\mathbf{K}(t) = (\cos\theta, \sin\theta)$, then $\mathbf{K}^+(t) = (\cos(\theta + \Delta\theta), \sin(\theta + \Delta\theta))$. The above form for $\hat{R}$ implies that $\cos\Delta\theta$ is a random variable with a uniform distribution on an interval I, where $I = [-1, 1]$ if $|\mathbf{k}_0| > 2M$, and $I = [1 - \frac{|\mathbf{k}_0|^2}{2M^2}, 1]$ if $|\mathbf{k}_0| \leq 2M$. In two space dimensions, the expression of the scattering coefficient Σ in (13) for the above choice of $\hat{R}$ in (25) is given after some algebra by

$$\Sigma(k) = \frac{c_0 k^3 \hat{R}_0}{4\pi} \begin{cases} \pi & \text{for} \quad k < \dfrac{M}{2} \\ \arccos\left(1 - \dfrac{M^2}{2k^2}\right) & \text{for} \quad k > \dfrac{M}{2}, \end{cases} \tag{26}$$

while we have for the diffusion coefficient in (17) the following expression

$$D(k) = \frac{c_0^2}{2(\Sigma(k) - \lambda(k))}, \tag{27}$$

where the anisotropy factor λ is given by

$$\lambda(k) = \frac{c_0 k^3}{4\pi} \begin{cases} 0 & \text{for} \quad k < \dfrac{M}{2} \\ \dfrac{\hat{R}_0\, M}{2\, k} \sqrt{1 - \dfrac{M^2}{4k^2}} & \text{for} \quad k > \dfrac{M}{2}. \end{cases} \tag{28}$$

Diffusion solver. The diffusion equation (16) on Ω is solved by a standard finite element method. Its initial condition is obtained from that for the transport equation via (16). It remains however to specify boundary conditions. It is well known that appropriate boundary conditions to model escape of energy at the domain boundary (through the perfectly matched layer in our simulations) are of the form [4,17]

$$U + 2L_2 D(k) \frac{\partial U}{\partial \boldsymbol{\nu}} = 0, \tag{29}$$

where L_2 is an extrapolation length in two space dimensions and $\boldsymbol{\nu}$ the normal unit vector at the boundary of the domain. In the case of isotropic scattering (i.e., $M = 2k$ above so that $\lambda(k) = 0$ and $l = l^*$), an approximate value for $L_2 = 0.81$ [4].

Treatment of the inclusion. One of the main objectives of this paper is to assess the validity of the radiative transfer equation when local (at the transport scale) modifications arise in the power spectrum of the random fluctuations. We consider two types of inclusions: (i) void inclusions where the randomness is suppressed so that $\hat{R}(\mathbf{x}, \mathbf{k}) = 0$ on the support of the inclusion (whence $\Sigma = 0$ and $D = \infty$ inside the inclusion) and; (ii) perfectly reflecting inclusions, where the inclusion is modeled by vanishing pressure for the wave code, specular reflections at the inclusion's boundary for the transport code, and Neumann boundary conditions at the same boundary for the diffusion approximation.

Such inclusions are easily incorporated into the wave and diffusion solvers. We need to be a little more careful to incorporate them into the transport code. The process $(\mathbf{X}(t), \mathbf{K}(t))$ described above is modified as follows in the presence of inclusions. In case (ii), the free transport between

collisions with the underlying medium is simply replaced by a specularly reflecting collision when the particle hits the inclusion's boundary (i.e., $\mathbf{K}(t)-\mathbf{K}^+(t)$ is proportional to the normal $\mathbf{n}(\mathbf{X}(t))$ at $\mathbf{X}(t)$ on the inclusion's boundary). In case (i), the free transport between collisions and the times of collisions are not changed. However at a time of collision, if $\mathbf{X}(t)$ is inside the collision, we set $\mathbf{K}^+(t) = \mathbf{K}(t)$ with probability one. We can verify that the probabilistic representation (24) holds in all cases.

In the Monte Carlo simulations of cases (i) and (ii) and their comparisons with the simulations in the absence of an inclusion, the statistical error caused by the law of large numbers is quite large compared to the influence of the inclusion on the measurements, unless a number of particles much larger than 10^6 is used. The solution to this problem is to solve the problems with and without inclusions (let us denote by (o) the case without an inclusion) using the same realizations of the random processes $(\mathbf{X}(t), \mathbf{K}(t))$ as much as possible. Let D_i be the spatial domain of the inclusion. Then (24) can be recast as

$$\begin{aligned}\int_A \int_B a(t,\mathbf{x},|\mathbf{k}_0|\hat{\mathbf{k}}) d\hat{\mathbf{k}} d\mathbf{x} = {} & \mathbb{P}\Big((\mathbf{X}(t),\mathbf{K}(t)) \in A\times B \,|\, \mathbf{X}(s)\in D_i \text{ for some } 0<s<t\Big) \\ & + \mathbb{P}\Big((\mathbf{X}(t),\mathbf{K}(t)) \in A\times B \,|\, \mathbf{X}(s)\notin D_i \text{ for all } 0<s<t\Big).\end{aligned} \tag{30}$$

The second contribution is obviously the same for cases (o), (i), (ii). In our evaluations of the differences (o)−(i) and (o)−(ii), it therefore vanishes. It still need be evaluated since we do not know a priori how many particles will reach D_i and when they will do so. However, the statistical fluctuations generated by this contribution are in many interesting cases at least as large as the other contribution in (30). It is therefore quite an efficient variance reduction method to estimate it for all cases (o), (i), and (ii) at once. The first contribution is estimated separately for all cases: as soon as a particle hits D_i, it branches out into three different particles, one for each case of interest.

Corrections due to the discretization. The kinetic model (12) concerns the continuous wave equation (1) and does not account for possible discretization effects. The corrections imposed by discretizations of the wave equations on the kinetic models were investigated recently in [3]. Two main effects need to be considered: first the group velocity is modified; this is a well known result; see e.g. [16]. Second, the kinetic parameters σ and Σ need be updated. The discrete group velocity is given by $\nabla_{\mathbf{k}} w(\mathbf{k})$ and the corrected mean free time by $\widetilde{\Sigma}^{-1} = \Sigma^{-1}(\mathbf{k})|R'(iw(\mathbf{k}))|^{-2}$ where $\Sigma^{-1}(\mathbf{k})$ is the continuous mean free time. Here, w is given by the dispersion relation of the 2nd order in space and time mixed formulation scheme of the acoustics wave equation,

$$\sin^2 \frac{w\Delta t}{2} = \left(\frac{c\Delta t}{2h}\right)^2 \left(\sin^2 k_x h + \sin^2 k_y h\right), \tag{31}$$

and $R(iw)$ is the symbol of the temporal discretization:

$$R(iw) = i\,\frac{2\,\sin\frac{w\Delta t}{2}}{\Delta}.$$

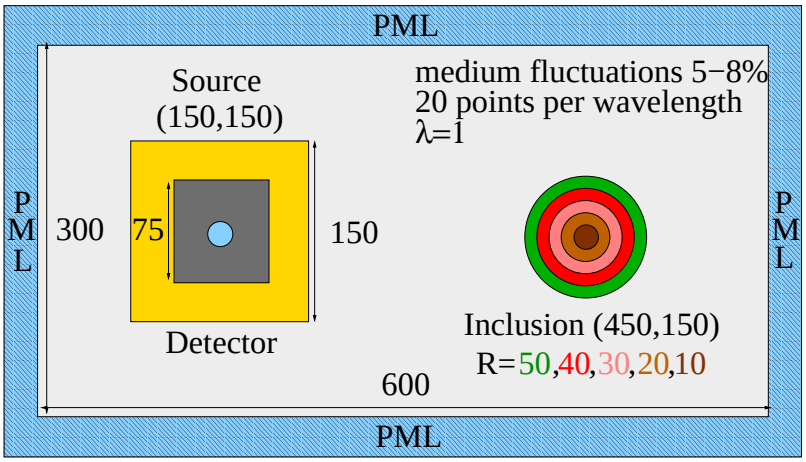

Fig. 1. Geometry of the problem for the parameter estimations.

Here, h is the spatial mesh and Δ the time step. A Taylor expansion in (31) yields

$$w(\mathbf{k}) = c|\mathbf{k}| \left(1 - \frac{h^2}{6|\mathbf{k}|^2}(k_x^4 + k_y^4)\right) = c|\mathbf{k}| \left(1 - \frac{h^2|\mathbf{k}|^2}{6}\left(1 - \frac{2k_x^2 k_y^2}{|\mathbf{k}|^4}\right)\right).$$

Assuming that $k_x k_y = 0$ (as in one space dimension) to simplify, we obtain that $\nabla_{\mathbf{k}} w(\mathbf{k}) = c\hat{\mathbf{k}}(1 - \frac{h^2|\mathbf{k}|^2}{2})$. In the discretization we have chosen for the wave equation, we have $h = \lambda/20$, $|\mathbf{k}| = 2\pi/\lambda$ so that $\frac{h^2|\mathbf{k}|^2}{2} \approx 0.05$. The average sound speed is then not given by $c_0 = 1$ but rather by $c_{\text{num}} = 0.95$. Concerning the dispersion relation, we have that $R'(iw) = \cos\frac{w\Delta t}{2}$ so that $|R'(iw(\mathbf{k}))|^2 \approx 1 - \frac{w^2\Delta t^2}{2} \approx 0.984$ in our simulations since we have chosen $\Delta t = 0.03$ to satisfy the CFL condition [16]. The discretization thus results in a very slight increase of the mean free time, which can be neglected. However the change in the sound speed of 5% caused by the discretization was accounted for in the simulation of the radiative transfer equations, so that the particles are modeled by the following jump process $(\mathbf{X}(t), 0.95\mathbf{K}(t))$.

4 Numerical simulations

This section has two objectives. The first one is to reconstruct the mean free path (or equivalently the scattering coefficient Σ) and the transport mean free path (or equivalently the diffusion coefficient D). The second one is to predict the influence of spatially localized changes in the scattering properties on the measured intensity. More specifically we want to understand the effect of (i) the distance between the detectors and the localized changes; (ii) the size of the localized changes; and (iii) the size of the detectors on the statistical stability of the measurements.

The computational domain for the wave, transport, and diffusion solvers presented in the preceding section is shown in Fig. 1. We denote by $\mathcal{D}$ the domain where the detectors are located. In Fig. 1, $\mathcal{D} = \mathcal{D}_1$ refers to the *large* detector, a square of sides equal to 150 wavelengths, and $\mathcal{D} = \mathcal{D}_2$ refers to the *small* detector, a square of sides equal to 75 wavelengths. The energies predicted as a function of time at the array of detectors is given by

$$\mathcal{E}(t) = \int_{\mathcal{D}} \mathcal{E}(t,\mathbf{x}) d\mathbf{x} = \frac{1}{2}\int_{\mathcal{D}} \left(\kappa(\mathbf{x}) p^2(t,\mathbf{x}) + \rho(\mathbf{x})|\mathbf{v}(t,\mathbf{x})|^2\right) d\mathbf{x}, \tag{32}$$

$$\mathcal{A}(t) = \int_{\mathcal{D}}\int_{\mathbb{R}^2} a(t,\mathbf{x},\mathbf{k})\, d\mathbf{k}\, d\mathbf{x} = \int_{\mathcal{D}}\int_{S^1} a(t,\mathbf{x},\hat{\mathbf{k}}|\mathbf{k}_0|) 2\pi|\mathbf{k}_0|\, d\hat{\mathbf{k}}\, d\mathbf{x}, \tag{33}$$

$$\mathcal{U}(t) = \int_{\mathcal{D}} U(t,\mathbf{x},|\mathbf{k}_0|) d\mathbf{x}, \tag{34}$$

for the wave, transport, and diffusion solvers, respectively. The simplification in (33) occurs because the initial condition is concentrated on the shell $|\mathbf{k}| = |\mathbf{k}_0|$ as was explained in the preceding section.

As shown in Fig. 1, we consider two sizes of detector arrays, two sizes of random fluctuations (5% and 8% standard deviation), two types of random media (isotropic with $M = 2$ and anisotropic with $M = 1.15$ as defined in the preceding section), and several sizes of inclusions. The inclusions are either non-scattering inclusions (the random fluctuations in the sound speed vanish locally) or perfectly reflecting inclusions (with pressure imposed to be 0 for the wave solver, specular reflection imposed for the transport code, and vanishing Neumann boundary conditions imposed for the diffusion solver). We now compare the wave solutions with the radiative transfer and diffusion predictions for several combinations of the parameters we have just described.

4.1 Estimation of the background physical parameters

We first consider the reconstruction of the mean free paths l and l^*, or equivalently of the mean free time Σ^{-1} and the diffusion coefficient D, in the absence of an inclusion. Until further notice, the detector array is the large one: $\mathcal{D} = \mathcal{D}_1$. The numerical value of Σ^{-1} is obtained by minimizing the quantity $\|\mathcal{E} - \mathcal{A}\|_{L^2(0,T)}$, where $T = 3000$. To obtain a good accuracy in the Monte Carlo simulations, 5.10^6 particles are used in the simulation. The theoretical sound speed is $c_0 = 1$ and because of discretization effects, the numerical sound speed is $c_{\text{num}} = 0.95$. The standard deviation in the sound speed is fixed in this subsection to $\sqrt{R_0} = 5\%$. Here R_0 is defined, based on (8) and (25), as $(2\pi)^2 R_0 = \pi M^2 \hat{R}_0$, and measures the mean square fluctuation in the sound speed. The numerical value of the diffusion coefficient $D(|\mathbf{k}_0|)$ is estimated by minimizing $\|\mathcal{E} - \mathcal{U}\|_{L^2(t_0,T)}$, where t_0 is a parameter that accounts for the fact that the diffusion limit is not a correct approximation for short times.

Note that the standard deviation $\sqrt{R_0}$ is not a very meaningful parameter to describe wave propagation in the radiative transport regime. The above formulas show that, for $\hat{R}_0$ fixed, doubling M from $2|\mathbf{k}_0|$ to $4|\mathbf{k}_0|$ doubles the standard deviation though it has no effect on the mean free paths $l(|\mathbf{k}_0|)$ and $l^*(|\mathbf{k}_0|)$. However, for a given choice of M, the mean free paths are indeed proportional to the square of the standard deviation, and we will use this standard parameter as a gauge of disorder in the system.

In the configuration described above, the results for the energies at the array of detectors $\mathcal{E}(t)$, $\mathcal{A}(t)$, and $\mathcal{U}(t)$, where the latter two correspond to simulations with $\Sigma(|\mathbf{k}_0|)$, $D(|\mathbf{k}_0|)$, and L_2 obtained by best fit (see below), are shown on figure 2 in the case of an isotropic medium $M = 2|\mathbf{k}_0|$ and an anisotropic medium $M = 1.15|\mathbf{k}_0|$.

Isotropic power spectrum. We choose here $M = 2|\mathbf{k}_0|$ so that the cross section is isotropic, i.e., $\lambda(|\mathbf{k}_0|) = 0$ and $l = l^*$, and then $\Sigma(|\mathbf{k}_0|) = c_0|\mathbf{k}_0|^3\hat{R}_0/4$. The numerical estimation of the mean free time $\Sigma_{\rm num}^{-1}$ obtained by best fit of $\|\mathcal{E} - \mathcal{A}\|_{L^2(0,3000)}$ is given by $\Sigma_{\rm num}^{-1} = 88.5$. The relative error on the energies is 1.8%. The theoretical value with $c_0 = 1$ is given by $\Sigma_{\rm th}^{-1} = 83.0$. However corrected for the slower speed of propagation caused by the discretization, we find a "theoretical value" (for the discrete waves) of $\Sigma_{\rm th}^{-1} = 86.9$, which fits extremely well (by 2%) to the numerical estimation.

For the diffusion regime, we set $t_0 = 400$ and obtain for the best fit of $\|\mathcal{E} - \mathcal{U}\|_{L^2(400,3000)}$ the following values $D_{\rm num} = 43.2$ and $L_{2\rm num} = 0.80$. This is to be compared to the theoretical values $D_{\rm th} = c_0^2(2\Sigma)^{-1} = 39.6$ and $L_{2\rm th} = 0.81$ after correction for the sound speed $c_{\rm num} = 0.95$. The relative residual error between $\mathcal{E}$ and $\mathcal{U}$ is about 2.0%. The error between the estimated and theoretical values is thus around 8% for D and 2% for $L_{\rm ex}$. This gives a relatively accurate description of the diffusion coefficient and the extrapolation length knowing that the computational domain is less than 7 mean free paths large in the horizontal direction and less than 4 mean free paths large in the vertical direction.

Anisotropic power spectrum. We now choose $M = 1.15|\mathbf{k}_0|$ so that the cross section is anisotropic and then $\Sigma(|\mathbf{k}_0|) = c_0|\mathbf{k}_0|^3\hat{R}_0 \arccos(1 - M^2/(2k^2))/4\pi$. We obtain $\Sigma_{\rm num}^{-1} = 86.5$ for a relative error of 2.1% between $\mathcal{E}$ and $\mathcal{A}$. The theoretical value for the mean free time is $\Sigma_{\rm th}^{-1} = 68.98$. After correction for the modified sound speed, this yields a mean free time given by $\Sigma_{\rm th}^{-1} = 72.23$ for an error compared to the theoretical value of about 15%.

For the diffusion regime, we set $t_0 = 1900$. We obtain for the best fit of $\|\mathcal{E} - \mathcal{U}\|_{L^2(1900,3000)}$ (on the order of 5.9%) the values $D_{\rm num} = 80.2$ and $L_{2\rm ex} = 0.38$. The theoretical value for $D_{\rm th} = 55.88$. There is no analytic expression for L_2 in that case but the extrapolation length is supposed to stay close to the isotropic value of 0.81. The prediction for D is thus 50% off what one expects from theory. This result does not depend dramatically on the choice of the parameter t_0 and does not substantially improve if L_2 is fixed at 0.81.

In this situation, the transport mean free path $l^* = 2D \approx 110$ becomes quite large compared to the vertical size of the domain (more than a third). We thus do not expect the diffusion approximation to be very accurate because of the important leakage of energy at the domain boundary. The numerical simulations confirm this fact. Note that the estimation for the mean free path l is also less accurate than in the isotropic case. The explanation we believe is numerical. The power spectrum chosen in (25) with $M < 2$ is quite singular and is thus relatively difficult to simulate numerically. In the numerical simulations, the integrals appearing in the estimate of Σ in (13) are replaced by inaccurate numerical integrations for singular power spectra, which explains the (still relatively moderate) discrepancy between the theoretical and numerical predictions for the mean free path.

4.2 Effect of spatially localized inclusions

We now keep the best fit estimates (not the theoretical values) obtained above for the isotropic and anisotropic cases to assess the influence of small inclusions and of the size of the array

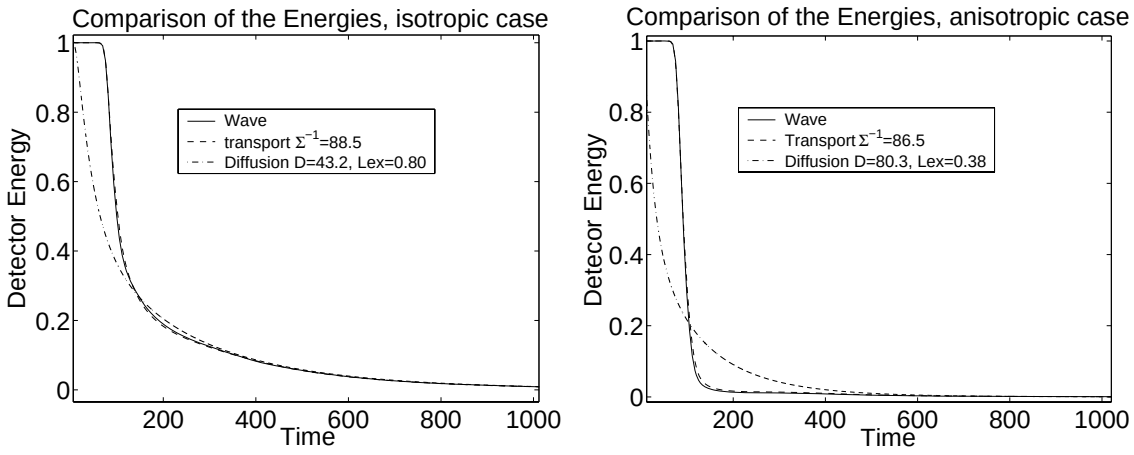

Fig. 2. Estimation of the parameters by comparison of the energies given by the wave, transport and diffusion models. Left: isotropic spectrum; Right: anisotropic spectrum.

of detectors on the energy density. As will become clear below, the fluctuations predicted by the wave and transport simulations are in quite a remarkable agreement. The fluctuations predicted by the diffusion model will only be valid when wave propagation really occurs in the diffusive regime.

The inclusion is modeled as a ball of radius R located at $\mathbf{x}_b$. It is characterized either by an absence of random fluctuations at its location and by an effective sound speed of $c_0 = 1$ (or $c_{\rm num} = 0.95$), as in the background medium, or by an infinite compressibility coefficient, which corresponds to a perfectly reflecting inclusion. At the transport level, the first type of inclusion is a collisionless zone. Within the diffusion regime, the inclusion is associated to either an infinite diffusion coefficient, as in [8], or to a vanishing diffusion coefficient, respectively.

The corrections caused by the inclusion are evaluated by the three numerical methods; $\mathcal{E}(t) - \mathcal{E}_{\rm inc}(t)$ by the wave solver; $\mathcal{A}(t) - \mathcal{A}_{\rm inc}(t)$ by the Monte-Carlo transport method, and $\mathcal{U}(t) - \mathcal{U}_{\rm inc}(t)$ by the diffusion method. Here, $\mathcal{E}_{\rm inc}(t)$, $\mathcal{A}_{\rm inc}(t)$ and $\mathcal{U}_{\rm inc}(t)$ refer to the energies measured at the array of detectors in the presence of the inclusion, which are subtracted to the corresponding energies obtained in the absence of an inclusion.

4.2.1 Void inclusion

We first consider the case of a void inclusion, where the random fluctuations in the sound speed are suppressed.

Isotropic power spectrum. In the case where $M = 2|\mathbf{k}_0|$, we plot the energy variations in Fig. 3 for the wave, transport, and diffusion solvers for two sizes of inclusions: $R = 40$ and $R = 50$. The inclusion is 300 (wavelengths) away from the source term and the center of array. The signal thus needs to propagate for at least $7l = 7l^*$ before it returns to the array of detectors after visiting the inclusion. We observe a very good agreement between the wave and transport predictions. The diffusive solution is not accurate for short times, but becomes quite accurate for relatively long times (close to $T = 3000$), as expected from theory.

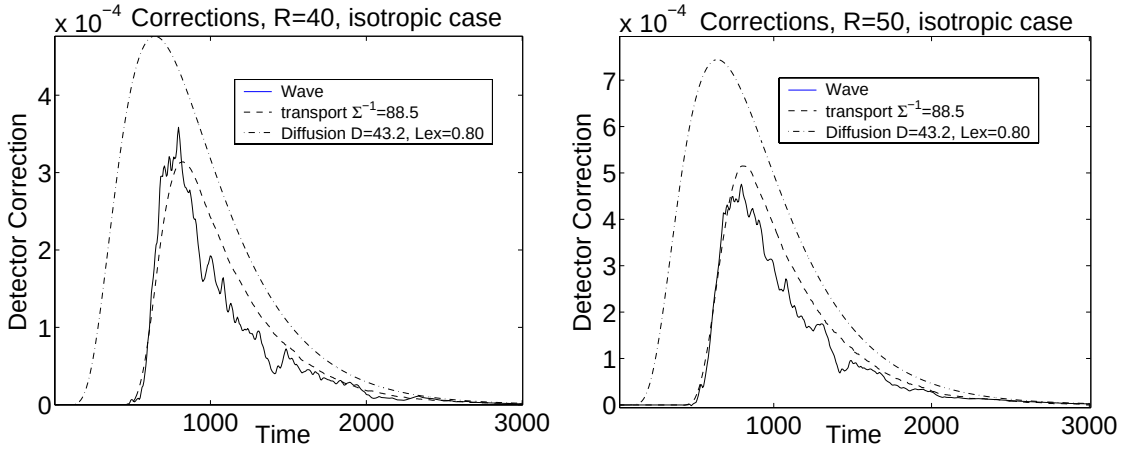

Fig. 3. Comparison of the corrections introduced by the perfectly homogeneous inclusion for the wave, transport, and diffusion models in the isotropic case. Left: $R = 40$; Right: $R = 50$.

Anisotropic power spectrum. We now consider the case where $M = 1.15|\mathbf{k}_0|$. The results

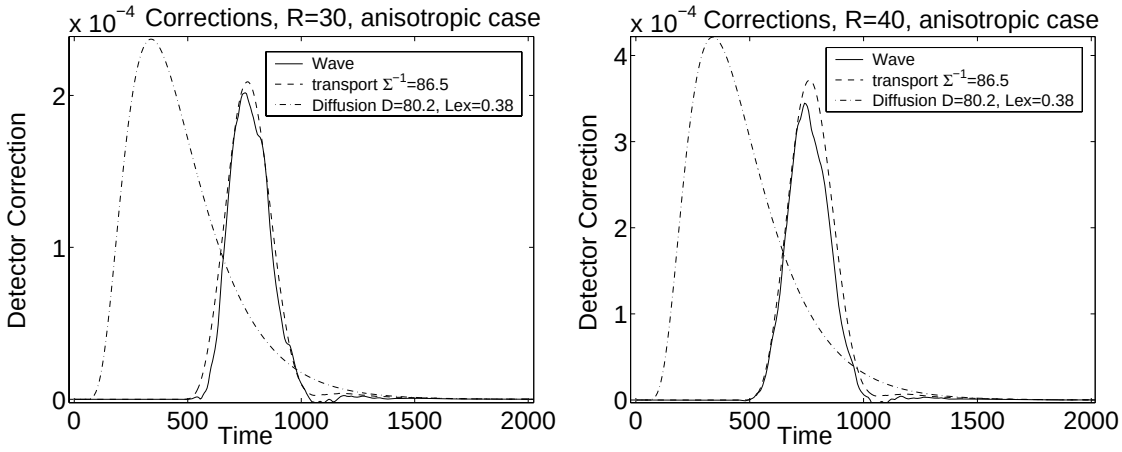

Fig. 4. Comparison of the corrections introduced by the perfectly homogeneous inclusion for the wave, transport, and diffusion models in the anisotropic case. Left: $R = 30$; Right: $R = 40$.

are shown in Fig. 4 for two sizes of inclusions: $R = 30$ and $R = 40$. The distance between the source/detectors and the inclusion is still on the order of $3.5l$ and roughly $2.7l^*$ (and less than $2l^*_{\text{num}}$, where $l^*_{\text{num}} \approx 160$, as estimated by the best diffusion fit). Since the diffusion approximation was not satisfactory in the absence of an inclusion, we do not expect to obtain a good fit between the diffusion and wave solvers. However, the transport solver still provides a remarkable estimate for the energy fluctuation.

Effect of increased random fluctuations. So far, $\sqrt{R_0}$ was set to 5%. We now increase this value to 8% in the case of isotropic fluctuations ($M = 2|\mathbf{k}_0|$), which has for effect to multiply the value of the mean free path by 2.56. The best fit estimates obtained in the absence of an inclusion by comparing wave, transport, and diffusion energy estimates, are given by $\Sigma^{-1}_{\text{num}} = 35$, $D_{\text{num}} = 17.0$, $L_{2\text{num}} = 0.79$, where we have chosen the final time of simulation $T = 4000$. The corresponding mean free paths are very close to being 2.56 times smaller than in the case of 5% of standard deviation for the fluctuations.

The variations in the energy density caused by the inclusion are presented in Fig. 5. Whereas transport simulations are very close to the wave energy predictions, now the diffusion solver also accurately predicts the energy variations. Note that the separation between the detectors and the inclusion is now roughly $8.5l = 8.5l^*$, so that by the time waves come back to the array of detectors (after propagating for $17l = 17l^*$ mean free paths), they essentially are diffuse waves. Note that because randomness in the system has increased substantially, the wave simulation becomes more oscillatory and less statistically stable. This effect will be further analyzed below.

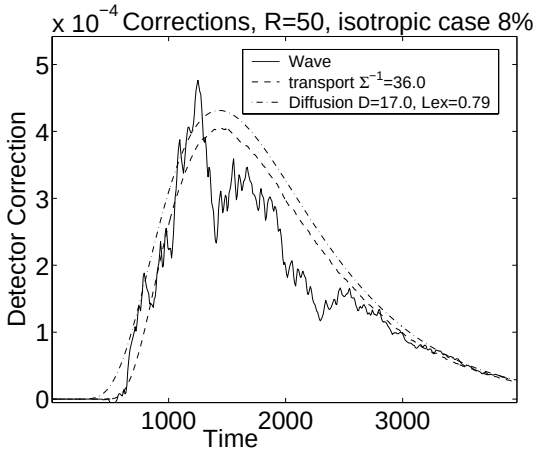

Fig. 5. Comparison of the corrections introduced by the perfectly homogeneous inclusion for the wave, transport, and diffusion solvers in the isotropic case with 8% fluctuations.

4.2.2 Perfectly reflecting inclusion

We now replace the void inclusion by a perfectly reflecting inclusion. It is modeled by vanishing pressure for the wave equation, by specular reflection at its outer boundary for the transport code, and by vanishing Neumann conditions at its outer boundary for the diffusion code. Note that in the diffusive regime, a void inclusion is modeled by a diffusion coefficient $D = \infty$ whereas a perfectly reflecting inclusion is modeled by a diffusion coefficient $D = 0$. We verify that in the limit of small inclusions (see e.g. [8, Eq. (22)]) the effect of a perfectly reflecting inclusion is the exact opposite of the effect of a void inclusion. The reason is simply that voids let as much energy propagate through as reflecting inclusions reflect back. We thus expect the variations $\mathcal{E}(t) - \mathcal{E}_{\rm inc}(t)$ to be non-positive.

Isotropic power spectrum. Let us consider the case of an isotropic power spectrum $M = 2|\mathbf{k}_0|$ and a standard deviation of 5% for the sound speed fluctuations. The results are shown in Fig. 6. Here again, wave and transport energy predictions agree quite well, whereas the diffusion approximation is valid only for long times.

Anisotropic power spectrum. We finally consider the case of an isotropic power spectrum $M = 1.15|\mathbf{k}_0|$ and a standard deviation of 5% for the sound speed fluctuations. The results are shown on figure 7 for two sizes of inclusions, $R = 20$ and $R = 30$. As in the case of a void inclusion, the diffusion solver does not capture the main aspects of the energy fluctuations. The transport model, however, is quite an accurate description of the wave energy fluctuations.

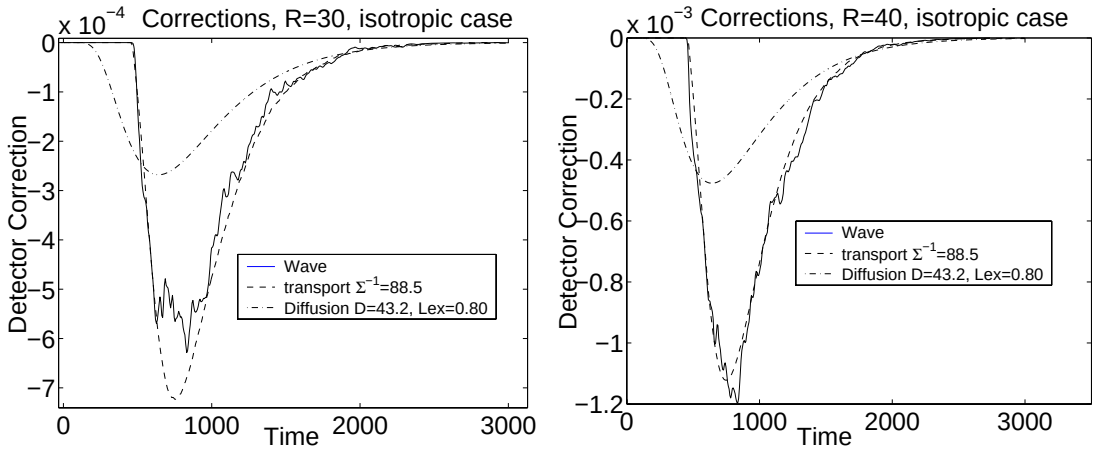

Fig. 6. Comparison of the corrections introduced by the perfectly reflecting inclusion for the wave, transport, and diffusion models in the isotropic case. Left: $R = 30$; Right: $R = 40$.

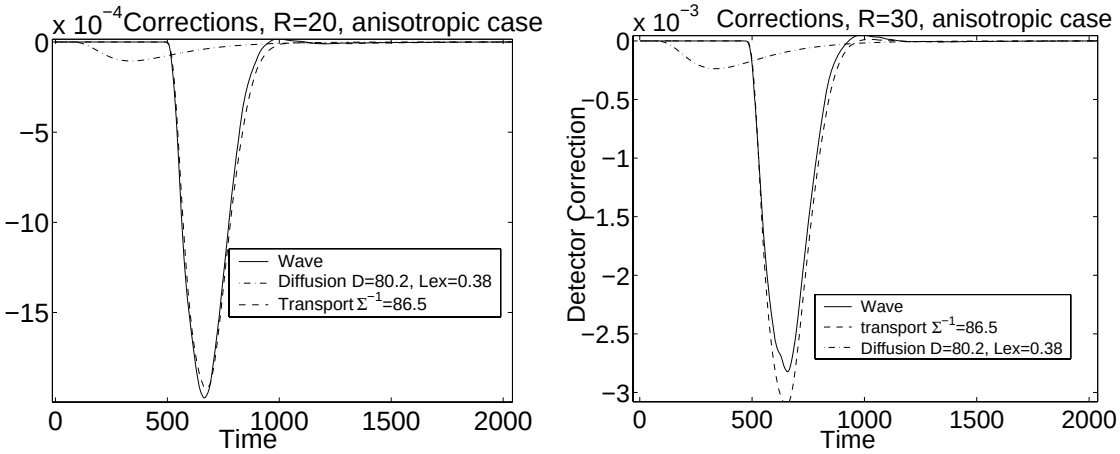

Fig. 7. Comparison of the corrections introduced by the perfectly reflecting inclusion for the wave, transport, and diffusion models in the anisotropic case. Left: $R = 20$; Right: $R = 30$.

4.3 Limitations of the radiative transport model

Radiative transfer equations offer a model for wave energy propagation over a fairly large range of regimes, including the weak coupling regime considered in this paper and the low density regime [20], where fluctuations are point scatterers that may be separated by distances orders of magnitude larger than the wavelength. In the regime of random Liouville, where the fluctuations have a correlation length much larger than the wavelength, the limiting behavior for the wave energy density is described by a Fokker-Planck equation [5], which can be seen as the highly-peaked forward approximation of the radiative transfer equation, and thus belongs to the same class of models (e.g. by sending M in (25) to 0 while appropriately rescaling the power spectrum). Radiative transfer is expected to be valid for random media with disorder that is not too large. As the transport mean free path converges to 0 (for very large fluctuations), the regime of wave localization is expected to arise [28]. Although we are not interested in this extremely high-disorder regime here, even moderately high disorder limits the applicability of radiative transfer.

The radiative transfer equation (12), as it is derived in e.g. [3,26] models the *average* wave energy density over realizations of the random medium. It remains to know how *stable* this prediction is with respect to changes in the realization for a given set of macroscopic statistical properties. The results obtained in simplified settings than radiative transfer in e.g. [2,7,10,24] show that the energy density is indeed statistically stable, at least provided that it is averaged over a sufficiently large detector. This is what we plan to investigate now.

Let us consider the case of the small detector $\mathcal{D} = \mathcal{D}_2$, which is a square of side equal to 75 wavelengths. Then in the case of isotropic fluctuations $M = 2|\mathbf{k}_0|$ and $\sqrt{R_0} = 5\%$, we observe that the wave energy captured on $\mathcal{D}_2$ is much more oscillatory than that on $\mathcal{D}_1$, in the case of a void inclusion of radius $R = 40$ and a perfectly reflecting inclusion of radius $R = 30$. We

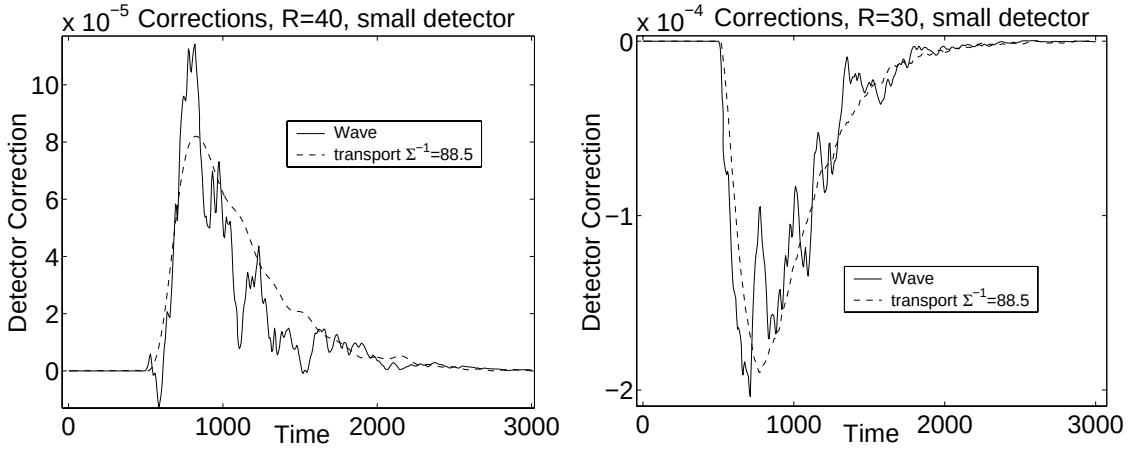

Fig. 8. Comparison of the corrections introduced by an inclusion for the wave and transport models in the isotropic case and with a small detector $\mathcal{D} = \mathcal{D}_2$. Left: void inclusion with $R = 40$; Right: reflecting inclusion with $R = 30$.

observe that the wave simulation is much more unstable than that in Figs. 3 and 6.

The above curves show the degradation of the radiative transfer prediction for smaller sizes of the array of detectors. The same phenomenon occurs if the size of the inclusion decreases. For instance, we show in Fig. 9 the energy fluctuations predicted by the wave and radiative transport models in the case of small void (with $R = 20$) or reflecting (with $R = 10$) inclusions. The radiative transfer still predicts the main features of the inclusion, for instance the sign of the fluctuation, and can thus be used for detection of inclusions. It may now however be too oscillatory (statistically unstable) to allow for a good prediction of the specific structure of the inclusion. For smaller radii of the inclusions than those in Fig. 9, even detection of the inclusion becomes questionable.

5 Conclusions

The main objective of this paper was to validate the theory of radiative transfer by comparing its wave energy predictions with simulations of wave propagation in random media. We have shown the quite remarkable agreement of the radiative transfer equations to model wave

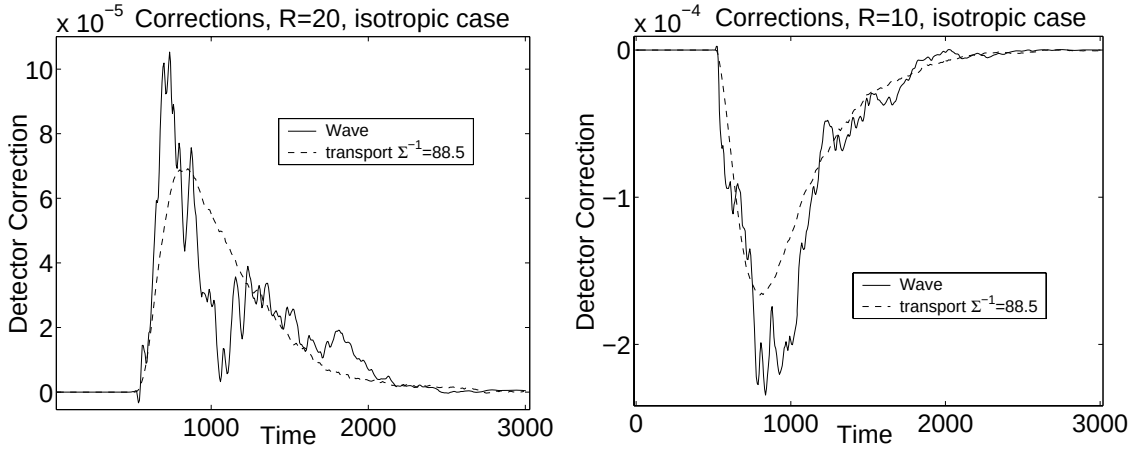

Fig. 9. Comparison of the corrections introduced by an inclusion for the wave and transport models in the isotropic case and with a large detector $\mathcal{D} = \mathcal{D}_1$ but small inclusions. Left: void inclusion with $R = 20$; Right: reflecting inclusion with $R = 10$.

propagation in the weak coupling regime, and to accurately predict the influence of localized modifications in the constitutive parameters of the transport equations, which here take the form of void or perfectly reflecting inclusions.

We have also quantified, on specific examples, the statistical stability of the radiative transfer model. For instance with $\sqrt{R_0} = 5\%$, inclusions separated from the radiation source by a little over $3l$ ($l \approx 90$) can be adequately predicted when measured over detectors of order $1.5l$ when their radius is more than $R = 0.25l$, with a similar result for inclusions with a radius twice as big when the detector side is twice as small. Such data provide valuable information for the detection and imaging of inclusions in cluttered media; see e.g. [8].

It would be interesting to simulate wave propagation on larger domains. For instance one expects that inclusions separated by a given number of mean free paths from a detector will generate more stable fluctuations when the standard deviation of the random fluctuations is halved. This in turn would require a domain of propagation four times larger counted in number of wavelengths. More numerical simulations are necessary to address such questions and will be done in the future.

Although our simulations are restricted to acoustic wave propagation, the results obtained in this paper should hold for more general wave phenomena, including quantum, electromagnetic, and elastic wave propagation [1,26]. It would however be quite interesting to see how accurately polarization effects in electromagnetic and elastic waves are predicted by the radiative transfer model. Such polarization effects are indeed quite useful to obtain properties of the random medium that intensity measurements alone can hardly predict [6].

Acknowledgment. This work was supported in part by DARPA-ONR grant N00014-04-1-0224 and NSF Grant DMS-0239097. GB also acknowledges support from the Alfred P. Sloan Fellowship.

References

[1] J. Achenbach, Wave propagation in elastic solids, North Holland, Amsterdam, 1991.

[2] G. Bal, On the self-averaging of wave energy in random media, Multiscale Model. Simul. 2(3) (2004) 398–420.

[3] G. Bal, Kinetic models for scalar wave fields in random media, to appear in Wave Motion.

[4] G. Bal, V. Freilikher, G. Papanicolaou, L. Ryzhik, Wave Transport along Surfaces with Random Impedance, Phys. Rev. B 62(10) (2000) 6228–6240.

[5] G. Bal, T. Komorowski, L. Ryzhik, Self-averaging of Wigner transforms in random media, Comm. Math. Phys. 242(1-2) (2003) 81–135.

[6] G. Bal, M. Moscoso, Polarization Effects of Seismic Waves on the Basis of Radiative Transport Theory, Geophys. J. Int. 142(2) (2000) 571–585.

[7] G. Bal, G. Papanicolaou, L. Ryzhik, Self-averaging in time reversal for the parabolic wave equation, Stochastics and Dynamics 4 (2002) 507–531.

[8] G. Bal, O. Pinaud, Time reversal-based imaging in random media, Inverse Problems 21 (2005) 1593–1620.

[9] G. Bal, L. Ryzhik, Time Reversal for Classical Waves in Random Media, C. R. Acad. Sci. Paris, Série I 333 (2001) 1041–1046.

[10] G. Bal, L. Ryzhik, Stability of time reversed waves in changing media, Disc. Cont. Dyn. Syst. A 12(5) (2005) 793–815.

[11] G. Bal, R. Verástegui, Time Reversal in Changing Environment, Multiscale Model. Simul. 2(4) (2004) 639–661.

[12] Y. Barabanenkov, A. Vinogradov, Kravtsov.Yu, V. Tatarskii, Application of the theory of multiple scattering of waves to the derivation of the radiative transfer equation for a statistically inhomogeneous medium, Radiofizika 15 (1972) 1852–1860. English translation pp. 1420–1425.

[13] J. P. Berenger, A perfectly matched layer for the absorption of electromagnetic waves, J. Comput. Phys. 114(2) (1994) 185–200.

[14] J. P. Berenger, Three-dimensional perfectly matched layer for the absorption of electromagnetic waves, J. Comput. Phys. 127(2) (1996) 363–379.

[15] S. Chandrasekhar, Radiative Transfer, Dover Publications, New York, 1960.

[16] G. C. Cohen, Higher-Order numerical methods for transient wave equations, Scientific Computation, Springer Verlag, Berlin, 2002.

[17] R. Dautray, J.-L. Lions, Mathematical Analysis and Numerical Methods for Science and Technology. Vol.6, Springer Verlag, Berlin, 1993.

[18] L. Erdös, H. T. Yau, Linear Boltzmann equation as the weak coupling limit of a random Schrödinger Equation, Comm. Pure Appl. Math. 53(6) (2000) 667–735.

[19] M. S. Howe, On the kinetic theory of wave propagation in random media, Phil. Trans. Roy. Soc. Lond. (274) (1973) 523–549.

[20] A. Ishimaru, Wave Propagation and Scattering in Random Media, New York: Academics, 1978.

[21] E. W. Larsen, J. B. Keller, Asymptotic solution of neutron transport problems for small mean free paths, J. Math. Phys. 15 (1974) 75–81.

[22] P.-L. Lions, T. Paul, Sur les mesures de Wigner, Rev. Mat. Iberoamericana 9 (1993) 553–618.

[23] L. Margerin, M. Campillo, B. A. van Tiggelen, Radiative Transfer and Diffusion of Waves in a Layered Medium: a New Insight into Coda Q, Geophys. Jour. Intern. 134(2) (1998) 596–612.

[24] G. Papanicolaou, L. Ryzhik, K. Sølna, Statistical stability in time reversal, SIAM J. App. Math. 64(4) (2004) 1133–1155.

[25] J. M. Powell, J. Vaneste, Transport equations for waves in randomly perturbed Hamiltonian systems, with application to Rossby waves, Wave Motion 42 (2005) 289–308.

[26] L. Ryzhik, G. Papanicolaou, J. B. Keller, Transport equations for elastic and other waves in random media, Wave Motion 24 (1996) 327–370.

[27] H. Sato, M. C. Fehler, Seismic wave propagation and scattering in the heterogeneous earth, AIP series in modern acoustics and signal processing, AIP Press, Springer, New York, 1998.

[28] P. Sheng, Introduction to Wave Scattering, Localization and Mesoscopic Phenomena, Academic Press, New York, 1995.

[29] J. Spanier, E. M. Gelbard, Monte Carlo principles and neutron transport problems, Addison-Wesley, Reading, Mass., 1969.

[30] H. Spohn, Derivation of the transport equation for electrons moving through random impurities, J. Stat. Phys. 17 (1977) 385–412.

[31] K. Watson, Multiple scattering of electromagnetic waves in an underdense plasma, Jour. Math. Phys. 10 (1969) 688–702.